International Journal of Minerals, Metallurgy and Materials
Volume 26, Number 5, May 2019, Page 588
https://doi.org/10.1007/s12613-019-1767-z

Effects of copper content on microstructure and mechanical properties of open-cell steel foams

Hamid Sazegaran[1)] *and Milad Hojati*[2)]

1) Department of Industrial Engineering, Faculty of Engineering, Quchan University of Technology, Quchan 94771-67335, Iran
2) Manufacturing Management of Mashhad Powder Metallurgy Company, Mashhad 94772-54258, Iran
(Received: 10 February 2018; revised: 20 November 2018; accepted: 22 November 2018)

Abstract: The effects of copper content on the microstructural and mechanical properties of steel foams are investigated. Spherical urea granules, used as a water-leachable space holder, were coated with a mixture of iron, ultrafine carbon, and different amounts of copper powders. After the mixture was compacted and the space holder was removed by leaching, a sintering process was performed under an atmosphere of thermally dissociated ammonia. Microstructural evaluations of the cell walls were carried out using optical microscopy and scanning electron microscopy in conjunction with energy-dispersive X-ray spectroscopy. In addition, compression tests were conducted to investigate the mechanical properties of the manufactured steel foams. The results showed that the total porosity decreases from 77.2% to 71.9% with increasing copper content in the steel foams. In the foams' microstructure, copper islands are mostly distributed in pearlite and intergranular carbide phases are formed in the grain boundaries. When the copper content was increased from 0 to 4wt%, the elastic modulus, plateau stress, fracture stress, and fracture strain of manufactured steel foams improved 4.5, 6, 6.4, and 2.5 times, respectively.

Keywords: steel foam; leachable space holder; copper content; liquid-phase sintering; mechanical properties

1. Introduction

Metallic foams and highly porous metals with cellular structures are a new class of advanced engineering materials [1–3]. These materials have very low specific weights, good physical and mechanical properties (e.g., high strength- and stiffness-to-weight ratios, good energy absorption capacity, good vibration dampening characteristics, and high gas permeability) in conjunction with good thermal properties [4–7]. The exclusive properties of cellular metals and metallic foams depend on the properties of the main alloy, porosity percentage, cell morphology (i.e., cell size and distribution, cell wall thickness, open or closed cells, and cell wall defects), and the operational factors of the manufacturing process [2–3].

Cellular metals and metallic foams are currently used in lightweight structural materials, automotive materials, aircraft materials, aerospace structural materials, impact energy absorbers, filters, and advanced power plant installations because of their exceptional properties [7–9]. Notably, steel foams are much more applicable than aluminum foams and other metallic foams because of the distinguished properties of steel. These properties include higher toughness, strength, stiffness, and heat resistance, lower cost, and better weldability compared with aluminum foams [10].

Cellular metals and metal foams are generally manufactured by the liquid metallurgy processes and powder metallurgy methods [1–2]. Because of their high melting point and complex control process, steel foams are more difficult to manufacture by the liquid metallurgy processes than by the powder metallurgy process. Highly porous steel parts and steel foams are therefore usually manufactured through powder metallurgy techniques [10–12]. Among the various processes of the powder metallurgy route, the most commonly used method is the space-holder technique. In this technique, a mixture of metal powders and an appropriate space-holder material are mixed and compacted; the space holder is then removed by heat treatment or a leaching process in an appropriate solvent. The process is followed by sintering under appropriate temperature and environ-

Corresponding author: Hamid Sazegaran E-mail: h.sazegaran@qiet.ac.ir

mental conditions for an appropriate time to manufacture the desired product [12–18].

In the space-holder technique, expanded polystyrene [19–20], magnesium [21], various salts [22–24], potassium carbonate [25], carbamide [14–16], urea [18,26], tapioca starch [27], and other materials are used for manufacturing metallic foams. Steel foams of 316L stainless steel and 17-4 PH stainless steel have been manufactured using angular and spherical carbamide and ammonium hydrogen carbonate particles as space holders [28–32]. In addition, ammonium bicarbonate and carbamide granules can be used as leachable materials to produce stainless steel foams and micro-alloyed steel foams, respectively [33–34].

In recent years, the manufacturing processes of steel foams have been widely investigated; however, the effects of adding various elements on the microstructure and mechanical properties of these steels have not yet been studied. In the present study, spherical urea granules coated with a mixture of commercial iron, ultrafine carbon, and copper powders are used to manufacture foams using the water-leachable space-holder technique. Furthermore, the effects of different amounts of copper on the porosity percentage, microstructure, and compression behavior of the manufactured steel foams are studied.

2. Experimental

2.1. Materials

Commercial water-atomized iron powder (purity >99.5%), commercial water-atomized copper powder (purity >99.9%), and ultrafine graphite powder (purity >99.99%), all supplied by Mashhad Powder Metallurgy Company, were used as raw materials. Although iron particles are irregular in shape, the size distribution is varied from 45 μm to 200 μm (Table 1 and Fig. 1(a)). In addition, the copper powder has an average particle size of 100 μm (Fig. 1(b)).

Table 1. Size distribution of iron particles wt%

160–200 μm	100–160 μm	63–100 μm	< 63 μm
3	30	31	36

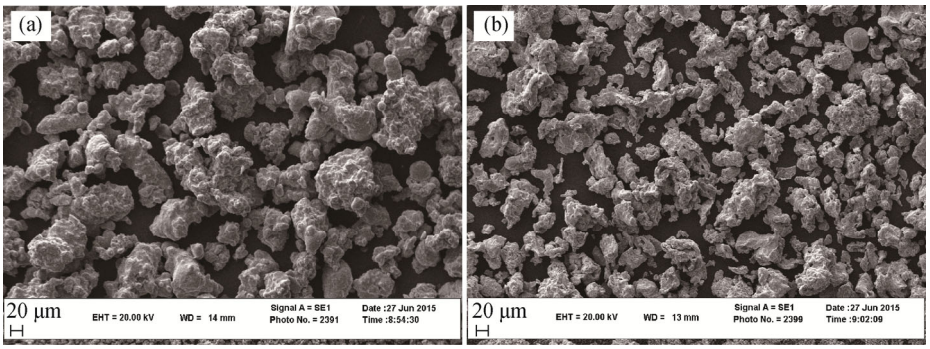

Fig. 1. SEM micrographs of iron (a) and copper (b) particles.

The iron powder was mixed with 1wt% of graphite powder, and 0, 1wt%, 2wt%, 3wt%, and 4wt% of copper powder in a blender (150 r/min, 30 min). Spherical urea granules (size: 1–1.5 mm, purity >99.5%, Merck) were selected as the water-leachable space-holder materials because of their very high water solubility.

2.2. Foaming technique

The main stages of the foaming process are: (1) preparation of the powder mixture; (2) coating of the urea granules with the powder mixture; (3) compacting the coated urea granules; (4) removing the space holder by leaching in distilled water; (5) sintering of the product. The main stages for manufacturing the steel foams are schematically shown in Fig. 2. First, the spherical urea granules were progressively poured into the cylindrical container of the mixer. Then, approximately 2wt% of distilled water was sprayed into the container and the surfaces of the urea granules were gradually wetted. Afterwards, the rotating process was carried out at 150 r/min for 1 min. As a result, the surfaces of urea granules became sticky because of interaction between the urea granules and the sprayed water. In the next stage, the mixture of powders was added to the mixer container and the mixing process was carried out at 150 r/min for an additional 2 min. Finally, the coated granules were dried in an oven at 50°C for 5 h. In this stage, the urea/powder weight ratio was selected as 1.

Next, the coated urea granules were cold compacted in a cylindrical stainless steel die (d = 12 mm and h = 100 mm). For the compaction process, the applied pressure selected to fabricate the green compacted specimens was 150 MPa [13]. The selection of an appropriate load ensures that the urea granules can be removed from the green compacted specimens without breaking them [14].

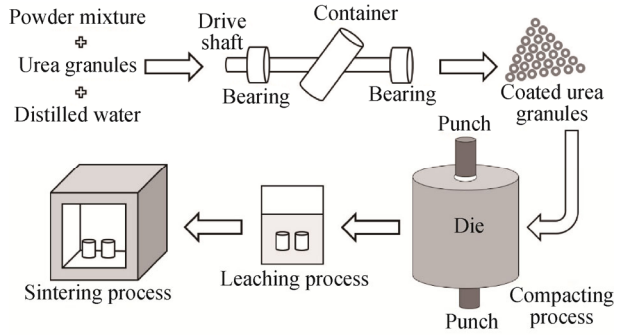

Fig. 2. Schematic stages of manufacturing the steel foams.

Afterward, the green compacted specimens were immersed in distilled water at 25°C for 2 h to leach the urea granules. The shape of the space holder can affect the time and temperature required during the leaching process. In a spherical space holder, in comparison with an irregular-shaped space holder, the formation of sharp, extended channels between the pores is restricted, leading to a longer leaching time [16,35]. In the leaching process, at least 90wt% of the urea granules were removed from the green compacted specimens. The leached specimens were then rinsed with ethanol and dried in oven at 50°C for 5 h. Steel foams were manufactured through the sintering of green specimens in a continuous furnace at 1120°C for 1 h under a dissociated ammonia atmosphere. The remaining urea was removed through thermal pyrolysis during the sintering process.

2.3. Density and porosity

The density of steel foams is defined as their mass per unit volume. The weight and volume of the specimens were determined using a digital balance and dimensional calculations, respectively. Therefore, the density of foams was obtained by dividing the weight of the foams by their volume. The porosity percentage of the steel foams was determined as [1]:

$$P = \left[1 - \left(\frac{\rho_F}{\rho_S}\right)\right] \times 100\% \quad (1)$$

where P is the porosity percentage, and ρ_F and ρ_S are the densities of the foam material and the solid bulk, respectively.

2.4. Microscopic evaluations

First, the steel foam specimens were mounted and polished in accordance with standard metallographic procedures. The cell morphologies of the manufactured steel foams and the microstructures of the cell walls were investigated using optical microscopy (OM) and scanning electron microscopy (SEM; LEO 1450VP). OM and SEM images were analyzed using microstructural image processing software (MIP^{TM}). In addition, the elemental composition and distribution in the cell walls were chemically characterized using energy-dispersive X-ray spectroscopy (EDS).

2.5. Mechanical properties

To study the influences of the additional amounts of copper on the mechanical properties, compression tests were conducted using a displacement-controlled universal testing machine (Zwick Z250) with a cross-head speed of 0.2 mm/min on compression specimens cut from sintered steel foams (d = 12 mm and h = 18 mm). For each manufactured steel foam, at least three specimens were mechanically tested.

3. Results and discussion

3.1. Cell morphology

The open-cell morphologies of the cylindrical 2wt% copper–steel foam specimen are reported in Fig. 3. The formation of open cells is common in metallic foams manufactured through the powder metallurgy technique using a leachable space holder [13–16]. The surface quality of the manufactured steel foams is very good, and little shrinkage is observed in the dimensions of the sintered specimen. Under a suitable applied pressure (150 MPa), the urea granules exhibited no damage. Furthermore, this applied pressure enabled easy subsequent leaching of the urea granules. As a result, interconnected open cells were consistently distributed, as observed in the images of the side surface (Fig. 3(a)) and top surface (Fig. 3(b)) of the sintered steel foam, and the cell walls continuously encircled the cells.

To investigate the distribution of internal cells and their intersected walls, steel foam specimens were accurately cut from the middle section and their surfaces were subsequently evaluated microscopically. The OM and SEM images of the internal cells and cell walls are presented in Fig. 4. The revealed open cells have reasonably spherical shapes in the horizontal and vertical cross sections. The various elliptical and spherical shapes of cells resulting from a higher applied pressure have been previously reported by other researchers [16,26]. In addition, two types of pores are observed in the steel foam specimens. One type (pore size between 1 and 1.5 mm) is related to the resolved urea granulates (Figs. 4(a) and 4(b)); the other type (average pore size ~35 μm) is formed between the agglomerated iron particles during the sintering process (Fig. 4(c)). Thus, the total porosity consists of the amounts of resolved urea cells and the pores in agglomerated particles (wall pores). The wall pores have relatively nonuniform, irregular shapes (Fig. 4(c)).

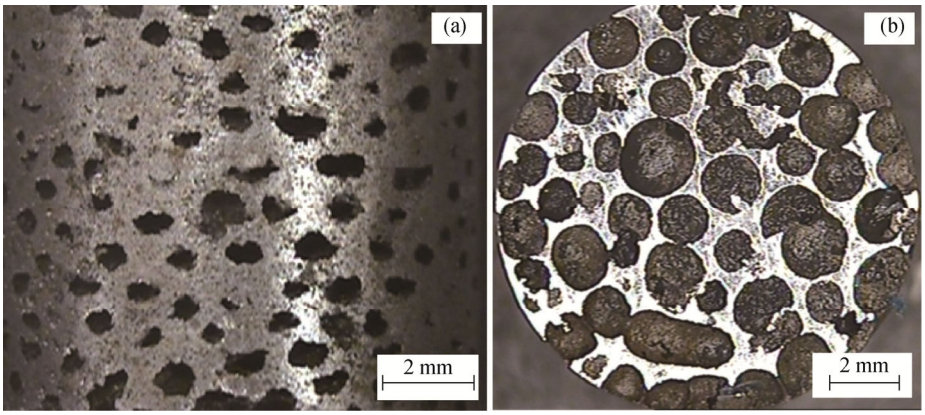

Fig. 3. Open cell morphologies of 2wt% copper-steel foam: (a) side view; (b) top view.

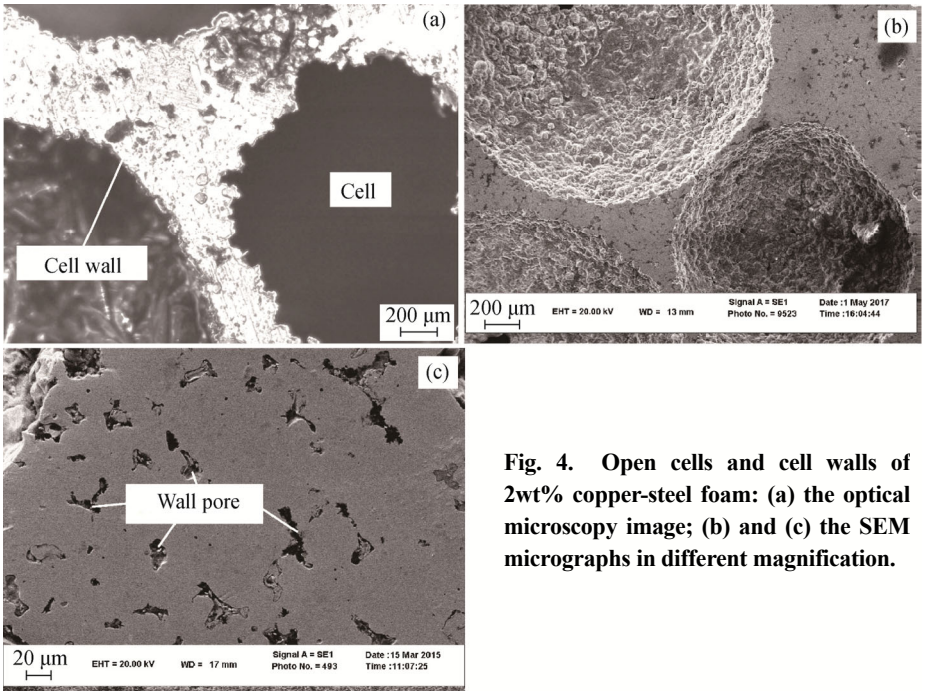

Fig. 4. Open cells and cell walls of 2wt% copper-steel foam: (a) the optical microscopy image; (b) and (c) the SEM micrographs in different magnification.

3.2. Porosity percentage

The surface fraction was measured from resolved urea cells and wall pores via analysis of OM and SEM images (Fig. 5). We observed that the surface fraction of wall pores decreased substantially with increasing amount of copper. This trend is attributed to the liquid-phase sintering process resulting from the addition of copper to the powder mixtures. In powder metallurgy steels, liquid-phase sintering can decrease porosity and increase densification in agglomerated iron particles through particle-rearrangement and solution-precipitation mechanisms [36–37]. Copper is known to be an effective element for liquid-phase sintering of powder metallurgy steels and to act as a bonding element during the sintering process [38–40]. Additional distributed copper in the mixtures melts at the sintering temperature (1120°C), which leads to thickening of the necks formed between sintered iron particles. Thus, the wall pores are substantially reduced. However, increasing the amount of copper in the cell walls of the manufactured steel foams can dramatically increase the liquid-phase sintering densification and reduce the surface fraction of the wall pores. Furthermore, no substantial difference was observed in the surface fraction of the resolved urea cells. The average value of the surface fraction for the resolved urea cells was 69.5%. In addition, the average measured thickness of the cell walls was approximately 250 µm.

The surface fraction of porosities and the volume fraction of porosities are approximately equal. Thus, the porosity percentage of manufactured steel foams can be calculated on the basis of the sum of the surface fraction of resolved urea cells and wall pores:

$$P_C = SF_{RUCs} + \left[(1 - SF_{RUCs}) \times SF_{WPs}\right] \quad (2)$$

where P_C is the calculated porosity percentage, and SF_{RUCs} and SF_{WPs} are the surface fractions of resolved urea cells and wall pores, respectively. A comparison between the measured porosity percentage (using Eq. (1)) and the calculated porosity percentage (using Eq. (2)) is illustrated in Fig. 6. This comparison reveals that the calculated values for porosity percentage are less than the measured amounts. Both the measured and the calculated porosity percentage decrease with increasing amount of copper in the mixture. This observation can explain the higher density of added copper in comparison with iron particles and the positive effects of copper on the densification [37].

3.3. Microstructure

SEM images of cell walls in the steel foam specimens are shown in Fig. 7. Wall pores and copper islands are randomly distributed in the microstructure (Fig. 7(a)). Under the experimental sintering conditions, because of imperfect diffusion, the copper particles melt and concentrate primarily on the external surfaces of the original iron particles. Furthermore, the molten copper fills some of the micropores between the iron particles. As a result, copper islands form between the original iron agglomerates, likely improving the mechanical properties of the manufactured steel foams by improving the bonding between the original iron particles. In addition, if the time of the sintering process is increased, then the copper islands may deform and grow, leading to enhancement of the mechanical properties [38–40].

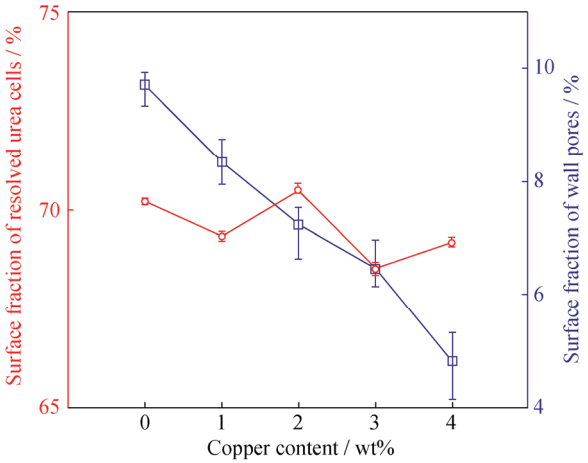

Fig. 5. Surface fraction of resolved urea cells and walls pores.

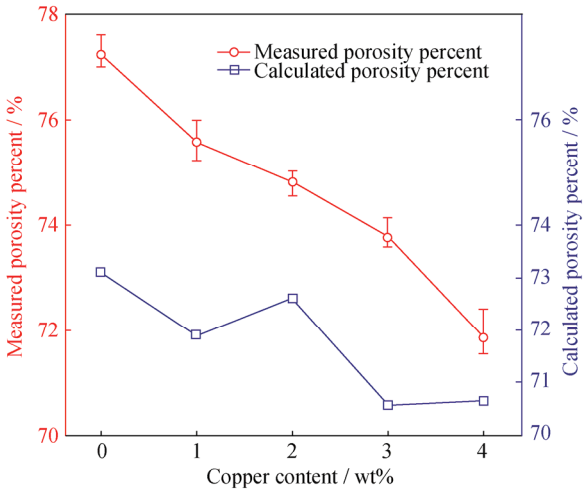

Fig. 6. Measured porosity percentage and calculated porosity percentage of manufactured steel foams.

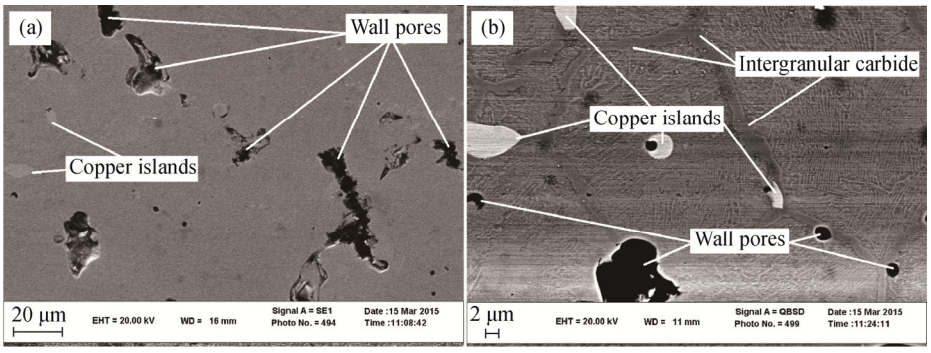

Fig. 7. SEM micrographs of cell walls in the 2wt% copper–steel foam specimen (a) and the 4wt% copper–steel foam specimen (b).

Scanning electron micrographs of steel foam specimens containing 0 to 4wt% Cu are shown in Fig. 8. The number of copper islands increases with increasing amount of added copper. In addition, intergranular iron carbide phases are formed in the grain boundary of the pearlite microstructure (Fig. 7(b) and Fig. 8). The formation of the intergranular iron carbide phases and the pearlite microstructure might be due to the diffusion of carbon during the sintering process.

A scanning electron micrograph of a cell wall of 2wt% copper–steel foam and the corresponding EDS results for different regions are shown in Fig. 9. EDS spectrum 1 includes Fe and Cu peaks (Fig. 9(b)). The peaks in EDS spectrum 2 (Fig. 9(c)) and EDS spectrum 3 (Fig. 9(d)) are attributable to Fe and C. Figs. 9(c) and 9(d) indicate that carbon diffuses into sintered iron agglomerates and forms iron carbide phases. Notably, the difference between EDS spectrum

2 and spectrum 3 is the amount of carbon. These investigations reveal three different microstructure regions: copper islands (Fig. 9(b)), intergranular iron carbide (Fig. 9(c)), and pearlite regions (Fig. 9(d)).

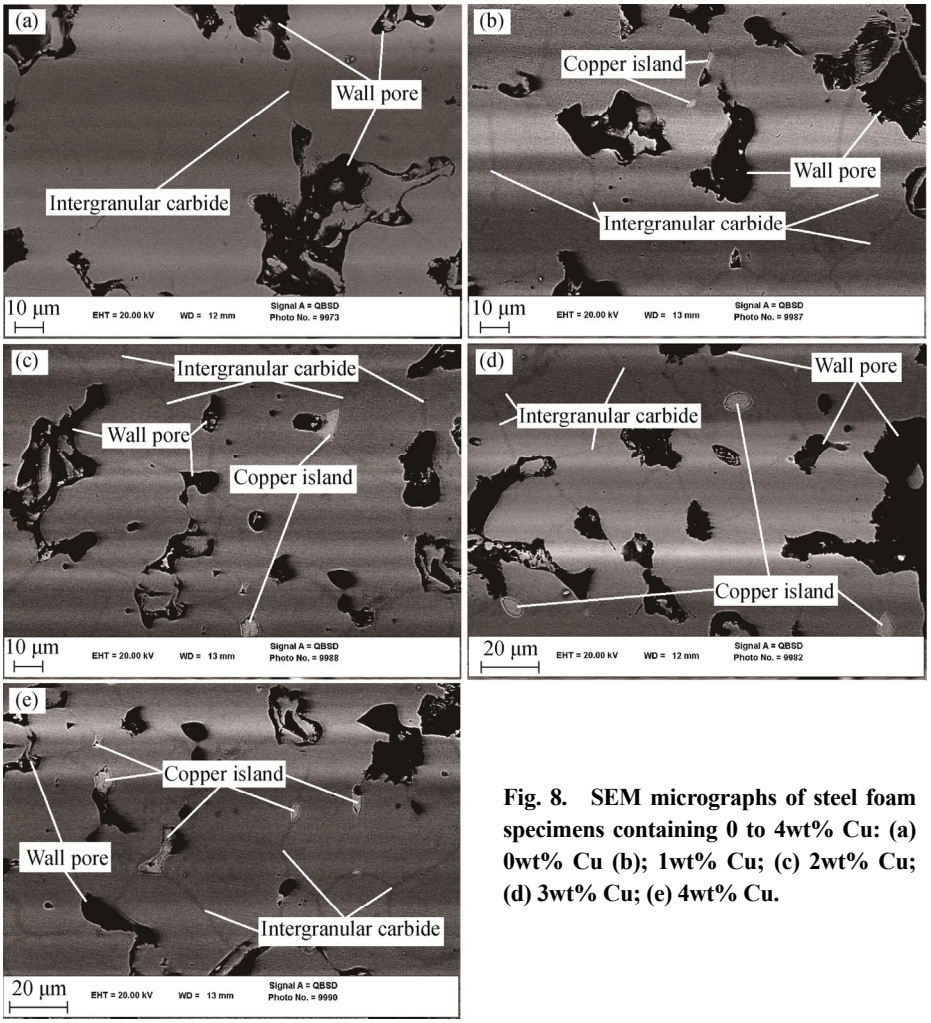

Fig. 8. SEM micrographs of steel foam specimens containing 0 to 4wt% Cu: (a) 0wt% Cu (b); 1wt% Cu; (c) 2wt% Cu; (d) 3wt% Cu; (e) 4wt% Cu.

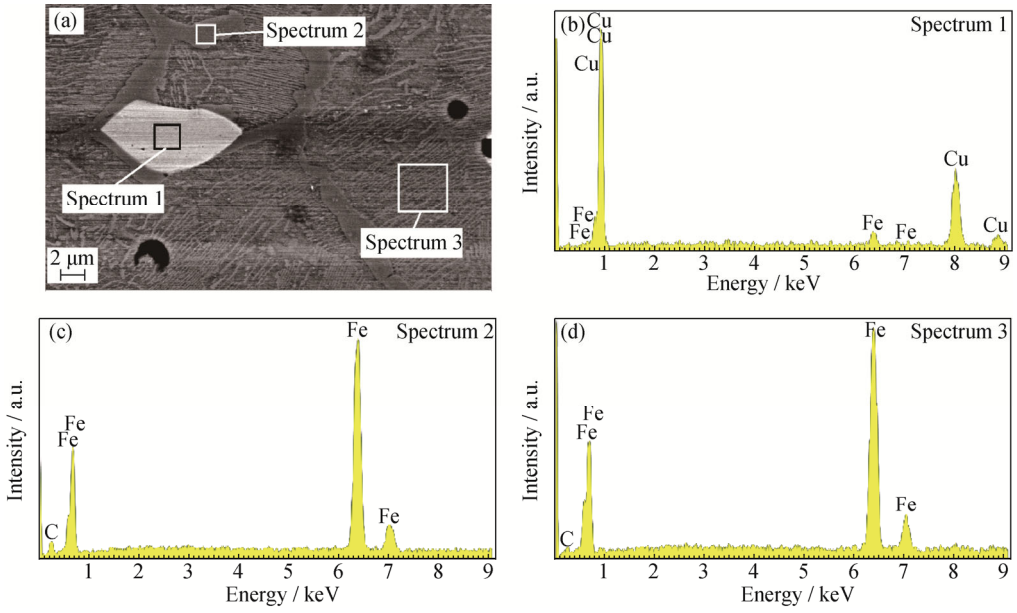

Fig. 9. SEM micrograph of a cell wall of 2wt% copper–steel foam specimen (a) and the corresponding EDS spectra of the different regions in (a): (b) copper island (spectrum 1); (c) intergranular iron carbide (spectrum 2); (d) pearlite region (spectrum 3).

3.4. Mechanical properties

The compressive stress vs. strain curves of the manufactured steel foams are depicted in Fig. 10. The foams demonstrate typical compressive stress vs. strain curves of metallic foams. They include an elastic deformation region, a plateau region, and a fracture point. Beyond the plateau region, the collapse region reported in other research works [14,16] is observed. The elastic region is almost linear and occurs at low stress values. The plateau region extends from the elastic region to the fracture point. With increasing amount of copper, the plateau stress and fracture strain increase considerably. In the steel foams with higher copper contents, a long region of saw-toothed plateau is observed. The formation of this region is related to the initiation and growth of microcracks in cell walls [14,34]. The collapse of cell walls in individual layers of cells causes a substantial reduction in the stress. As a result, a stress valley is clearly revealed in the stress–strain curves. The remaining cell walls then resist the applied stress. Therefore, a hill of stress is evidently formed in the curves. The sequences of hill-and-valley stresses resulting from the repeatable collapse of cell layers produce the long saw-toothed plateau region in the compressive stress–strain curves. We observed that the amount of copper can remarkably affect the size and shape of the hills and valleys in the plateau region. With an increase in the amount of copper, the height of the hills, the depth of the valleys, and their widths increase dramatically. The cell walls then contact each other, and the steel foams demonstrate bulk-like behavior under applied compressive stresses. Finally, brittle failure occurs at an angle of 45° relative to the applied compressive stress.

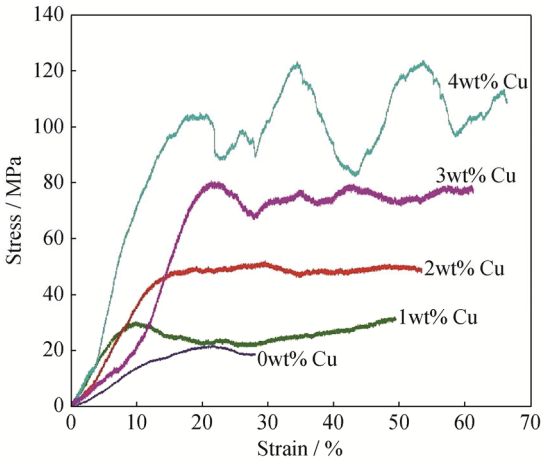

Fig. 10. Compressive stress vs. strain curves of manufactured steel foams.

Table 2 presents the obtained results of compressive stress–strain curves. The compressive properties are improved by increasing the amount of copper particles in the powder mixtures. In addition, the mechanical properties of the manufactured steel foams increase with increasing amount of added copper. Although the cell morphology (shape, size, and distribution of cells) and the porosity percentage strongly influence the mechanical behavior of the various metallic foams [41–43], liquid-phase sintering also influences the mechanical behavior of steel foams manufactured by powder metallurgy. As already discussed, adding copper particles to powder mixtures can improve the liquid-phase sintering process [38–40]. The liquid-phase sintering process increases the bonding between the iron particles, which in turn enhances the compressive properties of the foam. The improvement of the mechanical properties of aluminum foams through a liquid-phase sintering process has been previously reported [44–45].

Table 2. Elastic modulus, plateau stress, fracture stress, and fracture strain of manufactured steel foams

Copper / wt%	Elastic modulus / GPa	Plateau stress / MPa	Fracture stress / MPa	Fracture strain / %
0	0.12	17.2	17.6	26.8
1	0.42	23.7	28.7	48.6
2	0.38	45.9	47.1	54.2
3	0.46	72.6	74.8	62.8
4	0.54	104.8	112.5	67.6

4. Conclusions

In this study, high-porosity steel foams were successfully manufactured through the powder metallurgy technique by replication of urea granules as leachable space holders. The influence of various amounts of alloying element Cu on the microstructure and compressive properties of the manufactured steel foams was investigated, and the following conclusions are drawn:

(1) The manufactured steel foams have two types of porosity: one due to re-solvation of the urea granules during the leaching process, and the other one due to the formation of pores between agglomerated iron particles.

(2) The porosity percentage of steel foam was reduced by increasing the amount of copper.

(3) The measured porosity percentage was between 71.5% and 77.5%.

(4) The microstructure of the steel foam consists of distributed copper islands and intergranular carbides in pearlite.

(5) The stress–strain curves of the steel foams comprise an elastic region, a long saw-toothed plateau region, and a fracture point.

(6) With increasing amount of copper in the steel foam, its mechanical properties are generally improved.

References

[1] J. Banhart, Manufacture, characterization and application of cellular metals and metal foams, *Prog. Mater. Sci.*, 46(2001), No. 6, p. 559.

[2] M.F. Ashby, A.G. Evans, N.A. Fleck, L.J. Gibson, J.W. Hutchinson, and H.N.G. Wadley, *Metal Foams: A Design Guide*, Butterworth-Heinemann, 2000, p. 21.

[3] H.P. Degischer and B. Kriszt, *Handbook of Cellular Metals: Production, Processing and Applications*, Weinheim: Wiley-VCH/Verlag GmbH, 2002, p. 67.

[4] J. Baumeister, J. Banhart, and M. Weber, Aluminum foams for transport industry, *Mater. Des.*, 18(1997), No. 4-6, p. 217.

[5] K. Boomsma, D. Poulikakos, and F. Zwick, Metal foams as compact high performance heat exchangers, *Mech. Mater.*, 35(2003), No. 12, p. 1161.

[6] H.W. Song, Z.J. Fan, G. Yu, Q.C. Wang, and A. Tobota, Partition energy absorption of axially crushed aluminum foam-filled hat sections, *Int. J. Solids. Struct.*, 42(2005), No. 9-10, p. 2575.

[7] C. Motz and R. Pippan, Deformation behaviour of closed-cell aluminium foams in tension, *Acta. Mater.*, 49(2001), No. 13, p. 2463.

[8] S.V. Raj, L.J. Ghosn, B.A. Lerch, M. Hebsur, L.M. Cosgriff, and J. Fedor, Mechanical properties of 17-4PH stainless steel foam panels, *Mater. Sci. Eng. A*, 456(2007), No. 1-2, p. 305.

[9] J.Y. Seo, K.Y. Lee, and D.S. Shim, Effects of process parameters on properties of porous foams formed by laser-assisted melting of steel powder (AISI P21)/foaming agent (ZrH_2) mixture, *Opt. Laser. Technol.*, 98(2018), p. 326.

[10] B.H. Smith, S. Szyniszewski, J.F. Hajjar, B.W. Schafer, and S.R. Arwade, Steel foam for structures: A review of applications, manufacturing and material properties, *J. Constr. Steel. Res.*, 71(2012), p. 1.

[11] C. Park and S.R. Nutt, Effects of process parameters on steel foam synthesis, *Mater. Sci. Eng. A*, 297(2001), No. 1-2, p. 62.

[12] C. Park and S.R. Nutt, PM synthesis and properties of steel foams, *Mater. Sci. Eng. A*, 288(2000), No. 1, p. 111.

[13] M.H. Golabgir, R. Ebrahimi-Kahrizsangi, O. Torabi, H. Tajizadegan, and A. Jamshidi, Fabrication and evaluation of oxidation resistance performance of open-celled Fe(Al) foam by space-holder technique, *Adv. Powder Technol.*, 25(2014), No. 3, p. 960.

[14] N. Bekoz and E. Oktay, Effects of carbamide shape and content on processing and properties of steel foams, *J. Mater. Process. Technol.*, 212(2012), No. 10, p. 2109.

[15] N. Bekoz and E. Oktay, Effect of heat treatment on mechanical properties of low alloy steel foams, *Mater. Des.*, 51(2013), p. 212.

[16] M. Mirzaei and M.H, Paydar, A novel process for manufacturing porous 316L stainless steel with uniform pore distribution, *Mater. Des.*, 121(2017), p. 442.

[17] S. Guarino, M. Barletta, S. Pezzola, and S. Vesco, Manufacturing of steel foams by Slip Reaction Foam Sintering (SRFS), *Mater. Des.*, 40(2012), p. 268.

[18] M. Sharma, G.K. Gupta, O.P. Modi, B.K. Prasad, and A.K. Gupta, Titanium foam through powder metallurgy route using acicular urea particles as space holder, *Mater. Lett.*, 65(2011), No. 21-22, p. 3199.

[19] T. Shimizu, K. Matsuzaki, H. Nagai, and N. Kanetake, Production of high porosity metal foams using EPS beads as space holders, *Mater. Sci. Eng. A*, 558(2012), p. 343.

[20] J. Kadkhodapour, H. Montazerian, M. Samadi, S. Schmauder, and A.A. Mehrizi, Plastic deformation and compressive mechanical properties of hollow sphere aluminum foams produced by space holder technique, *Mater. Des.*, 83(2015), p. 352.

[21] E.E. Aşik and Ş. Bor, Fatigue behavior of Ti–6Al–4V foams processed by magnesium space holder technique, *Mater. Sci. Eng. A*, 621(2015), p. 157.

[22] G.Z. Jia, Y. Hou, C.X. Chen, J.L. Niu, H. Zhang, H. Huang, M.P. Xiong, and G.Y. Yuan, Precise fabrication of open porous Mg scaffolds using NaCl templates: Relationship between space holder particles, pore characteristics and mechanical behavior, *Mater. Des.*, 140(2018), p. 106.

[23] B. Xie, Y.Z. Fan, T.Z. Mu, and B. Deng, Fabrication and energy absorption properties of titanium foam with $CaCl_2$ as a space holder, *Mater. Sci. Eng. A*, 708(2017), p. 419.

[24] N. Takata, K. Uematsu, and M. Kobashi, Compressive properties of porous Ti–Al alloys fabricated by reaction synthesis using a space holder powder, *Mater. Sci. Eng. A*, 697(2017), p. 66.

[25] A. Noorsyakirah, M. Mazlan, O.M. Afian, M.A. Aswad, S.M. Jabir, M.Z. Nurazilah, N.H.M. Afiq, M. Bakar, A.J.M. Nizam, O.A. Zahid, and M.H.M. Bakri, Application of potassium carbonate as space holder for metal injection molding process of open pore copper foam, *Procedia. Chem.*, 19(2016), p. 552.

[26] B. Jiang, N.Q. Zhao, C.S. Shi, and J.J. Li, Processing of open cell aluminum foams with tailored porous morphology, *Scripta Mater.*, 53(2005), No. 6, p. 781.

[27] A. Mansourighasri, N. Muhamad, and A.B. Sulong, Processing titanium foams using tapioca starch as a space holder, *J. Mater. Process. Technol.*, 212(2012), No. 1, p. 83.

[28] H.I. Bakan, A novel water leaching and sintering process for manufacturing highly porous stainless steel, *Scripta Mater.*, 55(2006), No. 2, p. 203.

[29] M. Bram, C. Stiller, H.P. Buchkremer, D. Stöver, and H. Baur, High porosity titanium, stainless steel and superalloy parts, *Adv. Eng. Mater.*, 2(2000), No. 4, p. 196.

[30] H.Ö. Gülsoy and R.M. German, Sintered foams from precipitation hardened stainless steel powder, *Powder Metall.*, 51(2008), No. 4, p. 350.

[31] I. Mutlu and E. Oktay, Processing and properties of highly porous 17-4 PH stainless steel, *Powder Metall. Met. Ceram.*, 50(2011), No. 1-2, p. 73.

[32] I. Mutlu and E. Oktay, Production and aging of highly porous 17-4 PH stainless steel, *J. Porous Mater.*, 19(2011), No. 4, p. 433.

[33] D.P. Mondal, H. Jain, S. Das, and A.K. Jha, Stainless steel foams made through powder metallurgy route using NH_4HCO_3 as space holder, *Mater. Des.*, 88(2015), p. 430.

[34] N. Bekoz and E. Oktay, High temperature mechanical properties of low alloy steel foams produced by powder metallurgy, *Mater. Des.*, 53(2014), p. 482.

[35] N. Michailidis, F. Stergioudi, A. Tsouknidas, and E. Pavlidou, Compressive response of Al foams produced via a powder sintering process based on a leachable space-holder material, *Mater. Sci. Eng. A*, 528(2011), No. 3, p. 1662.

[36] R.M. German, P. Suri, and S.J. Park, Review: liquid phase sintering, *J. Mater. Sci.*, 44(2009), No. 1, p. 1.

[37] M.W. Wu, W.Z. Cai, Z.J. Lin, and S.H. Chang, Liquid phase sintering mechanism and densification behavior of boron-alloyed Fe–Ni–Mo–C–B powder metallurgy steel, *Mater. Des.*, 133(2017), p. 536.

[38] A. Simchi, Effect of C and Cu addition on the densification and microstructure of iron powder in direct laser sintering process, *Mater. Lett.*, 62(2008), No. 17-18, p. 2840.

[39] I. Metinöz, I. Cristofolini, I. Pahl, A. DeNicolo, P. Marconi, and A. Molinari, Theoretical and experimental study of the contact fatigue behavior of a Mo–Cu steel produced by powder metallurgy, *Mater. Sci. Eng. A*, 614(2014), p. 81.

[40] W.D. Wong-Ángel, L. Téllez-Jurado, J.F. Chávez-Alcalá, E. Chavira-Martínez, and V.F. Verduzco-Cedeño, Effect of copper on the mechanical properties of alloys formed by powder metallurgy, *Mater. Des.*, 58(2014), p. 12.

[41] U. Ramamurty and A. Paul, Variability in mechanical properties of a metal foam, *Acta Mater.*, 52(2004), No. 4, p. 869.

[42] Y.L. Mu, G.C. Yao, and H.J. Luo, Effect of cell shape anisotropy on the compressive behavior of closed-cell aluminum foams, *Mater. Des.*, 31(2010), No. 3, p. 1567.

[43] K. Essa, P. Jamshidi, J. Zou, M.M. Attallah, and H. Hassanin, Porosity control in 316L stainless steel using cold and hot isostatic pressing, *Mater. Des.*, 138(2018), p. 21.

[44] H. Bafti and A. Habibolahzadeh, Production of aluminum foam by spherical carbamide space holder technique-processing parameters, *Mater. Des.*, 31(2010), No. 9, p. 4122.

[45] Y.Y. Zhao, F.S. Han, and T. Fung, Optimisation of compaction and liquid-state sintering in sintering and dissolution process for manufacturing Al foams, *Mater. Sci. Eng. A*, 364(2004), No. 1-2, p. 117.